catalysts

MDPI

*Article*

# Photocatalytic Degradation of Vehicle Exhaust by Nano-$TiO_2$ Cement Slurry: Experimental Factors and Field Application

**Yachuan Kuang [1], Fuzheng Ding [1], Zhiwei Peng [1,*], Fan Fan [1], Zhaohuan Zhang [2] and Xiaoyong Ji [3]**

[1] School of Civil Engineering, Central South University, Changsha 410075, China; kuangyachuan@csu.edu.cn (Y.K.); dingfuzheng1026@163.com (F.D.); caihanghang981108@163.com (F.F.)
[2] Economic and Technical Research Institute of State Grid Shandong Electric Power Company, Jinan 250021, China; csutmy@163.com
[3] Traffic Construction Quality and Safety Supervision Bureau of Hunan Province, Changsha 410116, China; w1179458703@163.com
* Correspondence: pengzhiwei@csu.edu.cn

**Abstract:** Nano-$TiO_2$ combined with cement slurry can be utilized to degrade nitrogen oxides ($NO_x$) in vehicle exhaust, making it an excellent photocatalytic material for air purification. In practice, environmental factors can significantly affect the photocatalytic performance. In this study, a vehicle exhaust test system was developed, and the test methods and evaluation criteria for the degradation test are provided. This study investigated the photocatalytic degradation of $NO_2$ using nano-$TiO_2$ cement slurry through laboratory tests. The effects of temperature, relative humidity, ultraviolet (UV) radiation flux, cement slurry thickness, surface dust adherence, and the number of water rinsing cycles were examined. Additionally, nano-$TiO_2$ cement slurries were applied to an expressway toll station. The results showed that the efficiency of photocatalytic degradation was significantly influenced by temperature and UV radiation flux, while the thickness of the cement slurry had minimal impact. The photocatalytic degradation efficiency was negatively correlated to the relative humidity, when the relative humidity of the cement slurry specimens was high. This is because the excess water ($H_2O$) competes with $NO_2$ for adsorption. The photocatalytic performance of the samples was significantly reduced by surface dust and rain erosion, as both led to a decrease in the amount of nano-$TiO_2$ participating in the reaction. Furthermore, the photocatalytic material has wide-ranging potential applications. The findings of this study would support the promotion of environmentally friendly roads as a strategy to combat air pollution.

**Keywords:** nano-$TiO_2$ cement slurry; photocatalytic degradation; influencing factor; vehicle exhaust; field application

check for updates

**Citation:** Kuang, Y.; Ding, F.; Peng, Z.; Fan, F.; Zhang, Z.; Ji, X. Photocatalytic Degradation of Vehicle Exhaust by Nano-$TiO_2$ Cement Slurry: Experimental Factors and Field Application. *Catalysts* **2024**, *14*, 21. https://doi.org/10.3390/catal14010021

Academic Editors: Magdalena Janus and Bo Weng

Received: 10 December 2023
Revised: 23 December 2023
Accepted: 26 December 2023
Published: 27 December 2023

**Copyright:** © 2023 by the authors. Licensee MDPI, Basel, Switzerland. This article is an open access article distributed under the terms and conditions of the Creative Commons Attribution (CC BY) license (https://creativecommons.org/licenses/by/4.0/).

## 1. Introduction

With the prevalence of industrialization and urbanization, society has entered the automobile era. In 2020, the number of cars in China exceeded 200 million [1]. In addition, vehicle exhaust emissions account more than half of total nitrogen oxide ($NO_x$) emissions in some countries [2]. Vehicle exhaust emissions can reduce lung function, thereby increasing the risk of respiratory diseases [3–5]. $NO_x$ emitted from vehicle exhaust is a major contributor to air pollution, posing significant hazards to human health and the environment [6–9]. Furthermore, previous studies have suggested that nitrogen dioxide ($NO_2$) is linked to a higher occurrence of diabetes and cardiovascular diseases [10,11]. In addition to $NO_x$, carbon monoxide (CO) is another significant contributor to air pollution, leading to the greenhouse effect and acid rain [12–14]. Therefore, strict management of vehicle exhaust emissions is essential to protect the environment.

The management of vehicle exhaust has become a prominent issue worldwide. Currently, most methods focus on developing new energy sources and controlling engine exhaust to reduce the content of harmful substances in emissions. Hooftman et al. [15]

found that electric vehicles could have a positive impact on urban air quality, but they also noted the significance of their non-exhaust emissions. Venu et al. [16] combined nanoparticle-mixed palm biodiesel with exhaust gas recirculation, and the results showed that this new method could simultaneously reduce the emissions of harmful substances such as CO and $NO_x$. However, due to the rapid increase in vehicle ownership, the overall volume of harmful emissions remains substantial [17].

With the rapid development and popularization of photocatalytic technology, researchers are exploring the creation of new photocatalytic road materials to degrade vehicle exhaust. The catalytic degradation of vehicle exhaust is achieved by incorporating photocatalytic materials into pavements or auxiliary facilities. Nano-$TiO_2$ is an outstanding photocatalytic material capable of oxidizing harmful substances like CO, HC, and $NO_x$ from vehicle exhaust into environmentally friendly compounds such as $CO_2$, $H_2O$, and $HNO_3$ under ultraviolet (UV) light irradiation [18–21]. Nano-$TiO_2$ loaded on a cementitious material for purifying vehicle exhaust has been widely used [22–24]. In 2012 [25], a ~0.4 km photocatalytic concrete pavement was first paved in Louisiana, USA. Shen et al. [26] investigated $TiO_2$ as a catalyst in pervious concrete to promote a more environmentally friendly urban road infrastructure. Xia et al. [27] developed a visible light-responsive and durable photocatalytic coating based on water-based acrylic emulsion for the degradation of vehicle exhaust. Witkowski et al. [28] confirmed the effectiveness of photocatalytic concrete pavements for reducing nitrogen oxide (NO) based on the results of a field study in Warsaw. Wang et al. [29] utilized the photocatalyst g-$C_3N_4$ and nano-$TiO_2$ to modify the asphalt binder. The study findings showed that the photocatalyst had a significant ability to degrade NO.

Nano-$TiO_2$ has broad prospects in the field of organic and inorganic pollutant degradation, and the factors affecting the degradation efficiency in its application are worth exploring. Bhattu et al. [30] analyzed the efficient removal of emerging organic pollutants from water using various nanomaterials (NMs). Their findings indicated that NMs were a highly effective and easily synthesized solution for water remediation to address emerging pollutants. Das et al. [31] demonstrated the application of nanotechnology in soil, water, food, and air pollutants. Qian et al. [32] examined the influence of $NO_2$ concentration on the photocatalytic efficiency of $TiO_2$-loaded cement-base materials. Luo et al. [33] developed an environmentally friendly pervious concrete with photocatalytic properties that can enhance performance under both UV and sunlight. Jin et al. [34] discovered that the inclusion of Cu, Ce, and Fe significantly improved the photocatalytic degradation rate of NO and HC gases by $TiO_2$ pillared montmorillonite. Kuang et al. [35] investigated the optimal nano-$TiO_2$ doping, which was found to be 8–10% of the cement mass. Jin et al. [36] investigated the impact of $TiO_2$ pillared montmorillonite nanocomposites on the properties of matrix asphalt and their catalytic capacity for vehicle exhaust. Saber et al. [37] investigated the improvement of the photocatalytic activity of Au@$TiO_2$/rGO heterojunction nanocomposite under UV irradiation.

However, the study of how experimental factors affect the photocatalytic performance of nano-$TiO_2$ cement slurry is relatively incomplete. It is clear that nano-$TiO_2$ cement slurries need to be exposed to the external environment for the photocatalytic reaction to take place. Consequently, the potential problem of rainwater washout needs to be considered for practical applications. This is particularly important for the practical application of nano-$TiO_2$ cement slurry. Furthermore, few studies have combined indoor testing of nano-$TiO_2$ cement slurry with field applications. Another often overlooked issue is the selection of reliable metrics to accurately represent the degradation efficiency. Currently, most of the methods used to evaluate the efficiency of photocatalytic degradation of nano-$TiO_2$ cement slurry simply involve subtracting the initial reactant concentration from the concentration after the reaction [38–40]. However, these methods often overlook the adsorption of reactants by the nano-$TiO_2$ cement slurry itself.

In this study, we fabricated the nano-$TiO_2$ cement slurry using the ultrasonic dispersion method, developed a vehicle exhaust test system, and then determined a more accurate

degradation efficiency evaluation index. Subsequently, the impact of temperature, relative humidity, UV radiation flux, cement slurry thickness, dust accumulation on the surface, and the number of water rinses on the efficiency of $NO_2$ photocatalytic degradation by nano-$TiO_2$ cement slurry was investigated through indoor tests. Furthermore, we applied the nano-$TiO_2$ cement slurry at an expressway toll station and demonstrated its potential for application.

## 2. Mechanism of Nano-$TiO_2$ Cement Slurry Photocatalytic Degradation of Vehicle Exhaust

Nano-$TiO_2$ is a novel semiconductor material with a wide energy band gap and outstanding photocatalytic properties. Nano-$TiO_2$ has two energy bands: the conduction band (CB) and valence band (VB), which depend on whether they are filled with electrons ($e^-$). The energy gap between these two bands is called the forbidden band. Nano-$TiO_2$ exhibits photocatalytic properties when irradiated by UV light with energy greater than or equal to the forbidden bandwidth of 3.2 eV, corresponding to a wavelength of 387.5 nm or less [41–43]. In this case, electrons in the VB leap to the CB, forming holes ($h^+$) in the VB and hole–electron pairs with strong redox capabilities. When electrons are released from the surface of nano-$TiO_2$, they convert atmospheric oxygen into superoxide ions ($\cdot O_2{}^-$), which possess oxidizing properties, as shown in Equation (1). The superoxide ions further react to generate hydroxyl radicals (·OH) with strong oxidizing properties, as shown in Equations (2)–(4). Simultaneously, the $h^+$ also exhibit strong oxidation, allowing them to capture the electrons in $H_2O$ and $OH^-$ on the surface of the particles to produce ·OH radicals, as shown in Equations (5) and (6).

$$e^- + O_2 \rightarrow \cdot O_2^- \quad (1)$$

$$\cdot O_2^- + H_2O \rightarrow HOO\cdot + OH^- \quad (2)$$

$$2HOO\cdot \rightarrow H_2O_2 + O_2 \quad (3)$$

$$H_2O_2 + e^- \rightarrow \cdot OH + OH^- \quad (4)$$

$$H_2O + h^+ \rightarrow \cdot OH + H^+ \quad (5)$$

$$OH^- + h^+ \rightarrow H_2O \quad (6)$$

The $\cdot O_2{}^-$ ions and ·OH radicals catalyze the decomposition of harmful gases, as shown in Equations (7)–(9). The $NO_3{}^-$ ions generated by the reaction attach to the surface of the catalyst and are carried away when exposed to water. The nano-$TiO_2$ does not change because it is a photocatalyst. Figure 1 illustrates the mechanism of photocatalytic degradation of vehicle exhaust using nano-$TiO_2$ [44,45].

$$NO + 2\cdot OH \rightarrow NO_2 + H_2O \quad (7)$$

$$NO + \cdot O_2^- \rightarrow NO_3^- \quad (8)$$

$$NO_2 + \cdot OH \rightarrow HNO_3 \quad (9)$$

To expedite the development of eco-friendly roads, nano-$TiO_2$ can be incorporated in a precise manner into the cement slurry on the surface of pavements or auxiliary facilities, thereby achieving a purifying effect on vehicle exhaust. The rough and multi-void structure of the nano-$TiO_2$ cement slurry creates a highly concentrated vehicle exhaust field, which serves as an effective photocatalytic reaction site for nano-$TiO_2$, as illustrated in Figure 2 [22]. There are two stages in the photocatalytic degradation of $NO_x$ in vehicle exhaust by nano-$TiO_2$ attached to the surface of cement slurry. The first is that $NO_x$ is directly attached to the surface of nano-$TiO_2$, where $NO_x$ is oxidatively degraded by the $\cdot O_2{}^-$ and -OH generated on the surface of nano-$TiO_2$ by UV light. The second is that, after the $NO_x$ adhered to the surface of nano-$TiO_2$ is photocatalytically degraded, due to the rough multi-void structure of the cement slurry, the vehicle exhaust adsorbed on its surface gradually diffuses from

the high-concentration region to the low-concentration region, i.e., the surface of nano-$TiO_2$, and is then photocatalytically degraded by the concentration gradient effect. The coexistence of the two pathways greatly promotes the degradation efficiency of nano-$TiO_2$ cement slurry on vehicle exhaust.

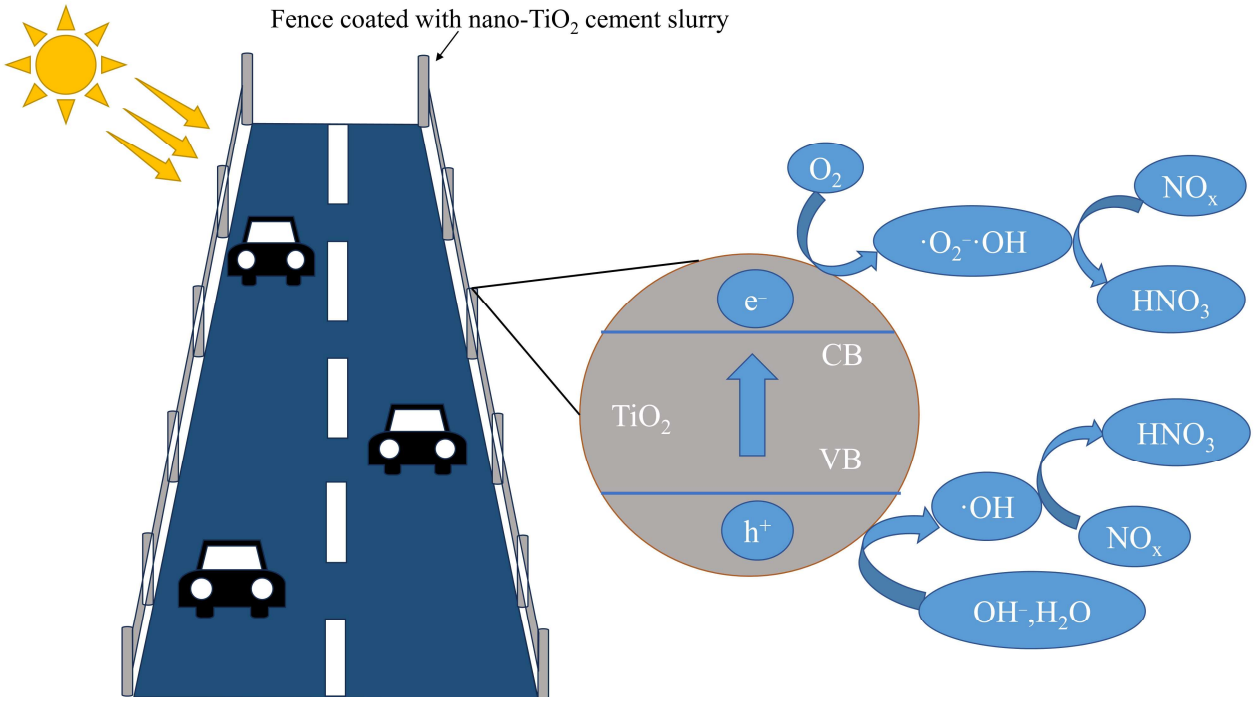



**Figure 1.** Mechanism of nano-$TiO_2$ photocatalytic degradation of vehicle exhaust.

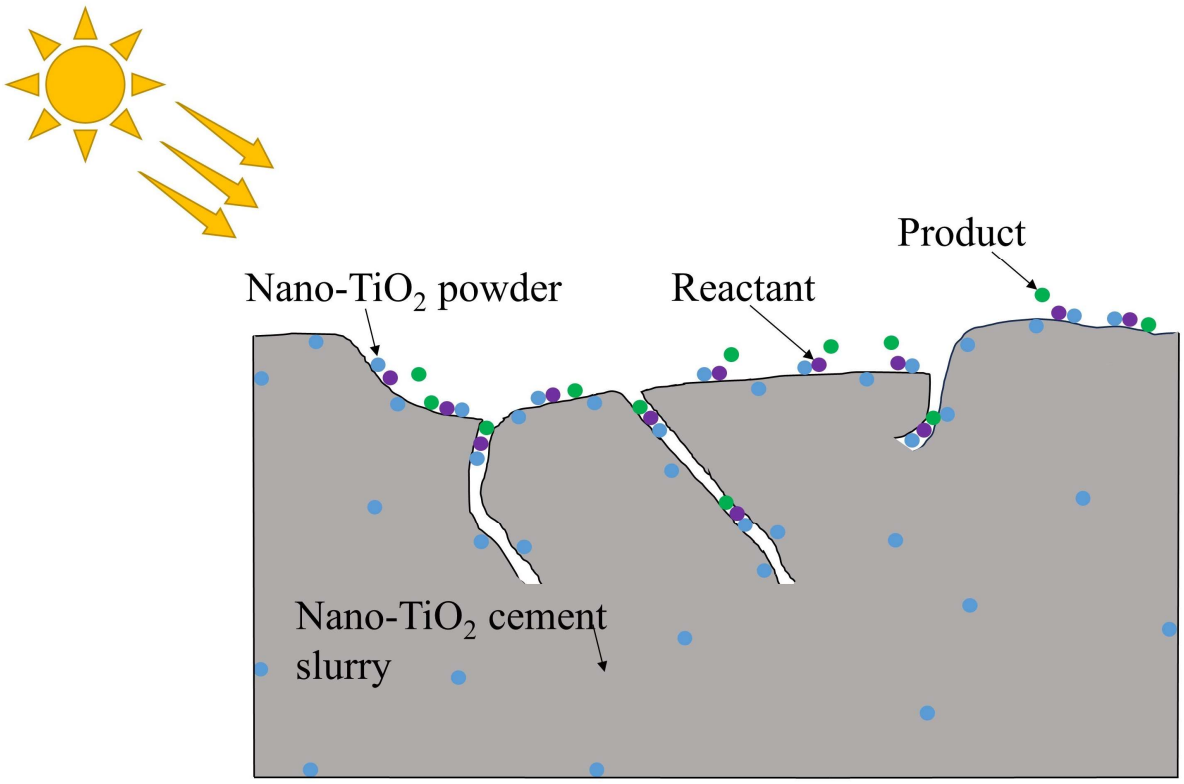



**Figure 2.** The photocatalytic reaction on the surface of nano-$TiO_2$ cement slurry.

## 3. Results and Discussions

### *3.1. Effect of Temperature*

Throughout the test, we activated the middle six UV lamps. Figure 3 vividly illustrates the influence of temperature on the efficiency of $NO_2$ photocatalytic degradation by nano-$TiO_2$ cement slurry. It can be observed that there was a maximum degradation efficiency of ~34.5% in the fitting curve, when the temperature was ~28.8 °C. Within the temperature range of 19.6–28.8 °C, the degradation efficiency increased as the temperature rose. However, as the temperature exceeded 28.8 °C, the degradation efficiency began to decline. The photocatalytic reaction is intricately linked to the diffusion and migration of reactant molecules on the catalyst surface [46,47]. During the initial heating stage, $NO_2$ molecules actively diffused and migrated on the surface of nano-$TiO_2$ cement slurry as the temperature rose, resulting in an increased degradation efficiency. However, when the temperature exceeded the optimal reaction temperature, excessively active $NO_2$ molecules detached from the nano-$TiO_2$ surface, subsequently leading to a reduction in the efficiency of $NO_2$ photocatalytic degradation by nano-$TiO_2$ cement slurry. Previous studies also found that there is an optimal reaction temperature for photocatalytic reactions. Above this temperature, the degradation efficiency no longer increases but gradually decreases [48,49].

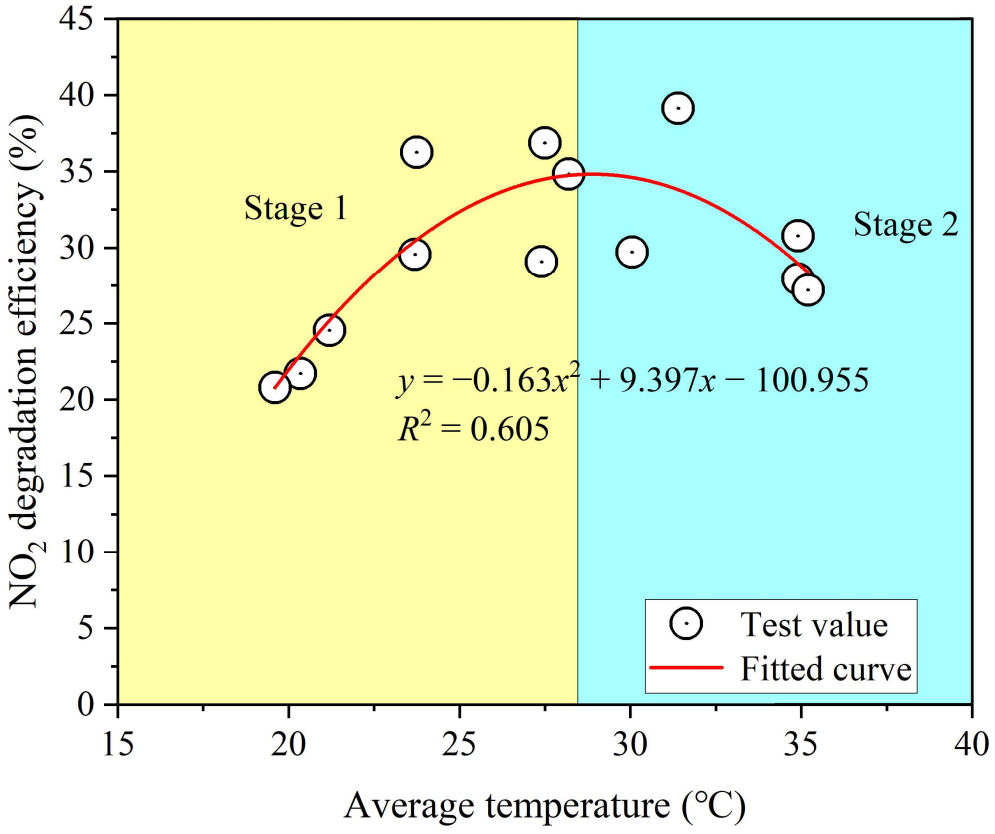



**Figure 3.** $NO_2$ degradation efficiency versus temperature.

### *3.2. Effect of Relative Humidity*

The relative humidity range in the test was 64.1–81.8%, due to the highest and lowest monthly average relative humidity in the Changsha region being 82% and 64%, respectively. As depicted in Figure 4, a total of 17 nano-$TiO_2$ cement slurry samples were immersed in water individually for 30 min. Subsequently, they were subjected to different drying times using drying equipment to attain various levels of relative humidity. The specimens were dried for durations of 0 h, 0.5 h, 1 h, 2 h, 3 h, 4 h, 5 h, 6 h, 7 h, 8 h, 9 h, 10 h, 13 h, 15 h, 18 h, 20 h, and 24 h, respectively.

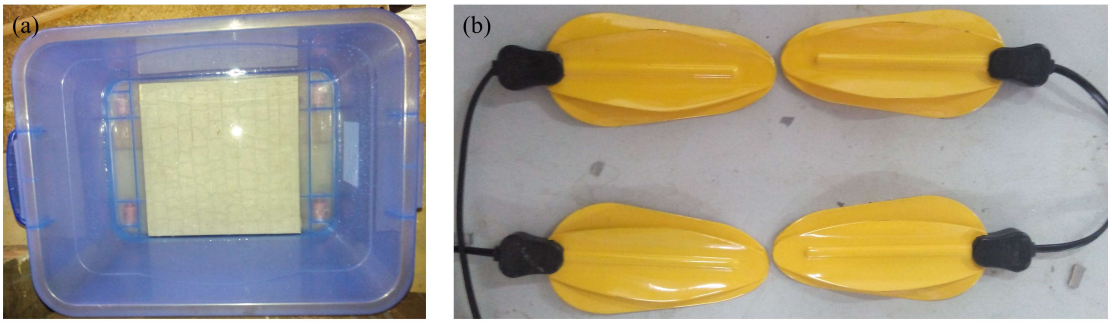



**Figure 4.** (**a**) Immersed cement slurry sample; (**b**) drying equipment.

The impact of relative humidity on the efficiency of $NO_2$ photocatalytic degradation by nano-$TiO_2$ cement slurry is shown in Figure 5. It is evident that the efficiency of $NO_2$ degradation decreased with an increase in relative humidity within the range of 64.1–81.8%. As $H_2O$ serves as a crucial reactant in the photocatalytic reaction, an increase in its concentration should theoretically enhance photocatalytic efficiency [50]. In the current experiment, we did not observe an upward trend within the range we investigated. These results may be attributed to the following factors. During the test, humidity levels ranged from 64.1% to 81.8%, potentially exceeding the optimal humidity for the reaction. As a reactant in the photocatalytic reaction, excess $H_2O$ would compete with $NO_2$ for adsorption at specific catalyst active sites in the nano-$TiO_2$. This inhibited the efficiency of $NO_2$ photocatalytic degradation by nano-$TiO_2$ cement slurry [51,52].

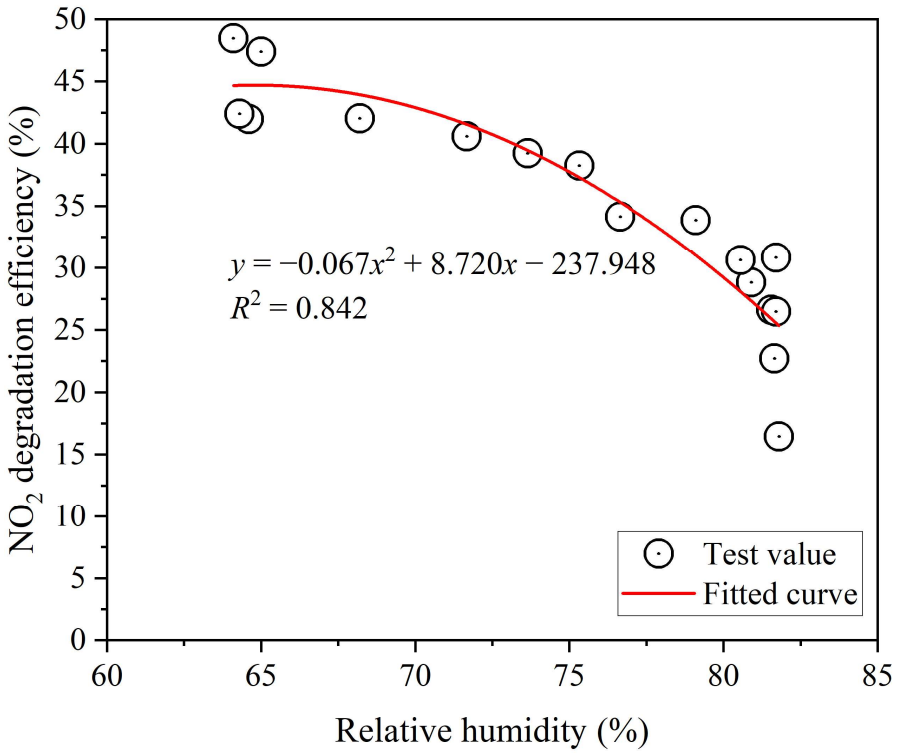



**Figure 5.** $NO_2$ degradation efficiency versus relative humidity.

### *3.3. Effect of UV Radiation Flux*

To precisely control the UV radiation flux applied to the nano-$TiO_2$ cement slurry, we exercised quantitative control by regulating the number of UV lamps activated in the reaction chamber. These UV lamps were sequentially numbered from 1 to 14 and positioned directly above the test specimens. The horizontal distance between the UV lamps on both

sides and the edge of the specimen was maintained at 40 mm. In Figure 6, we present UV lamp 1 as an illustrative example for the calculation model of UV radiation flux. The UV lamp was activated and abstracted as a linear light source. A Cartesian coordinate system was established, with the operating plane as the *xoy* plane. The two endpoints of the linear light source were $A_0$ and $B_0$, with coordinates ($x_0 + l_0$, $y_0$, $h_0$) and ($x_0$, $y_0$, $h_0$), respectively. M ($x_m$, $y_0$, $h_0$) was a moving point on line $A_0B_0$, and $P$ ($x$, $y$, 0) was a point on the working plane. The illumination of $M$ to $P$ was calculated using the irradiance calculation formula (Equation (10)):

$$E_{MP} = \frac{I \cos \alpha}{d^2} \tag{10}$$

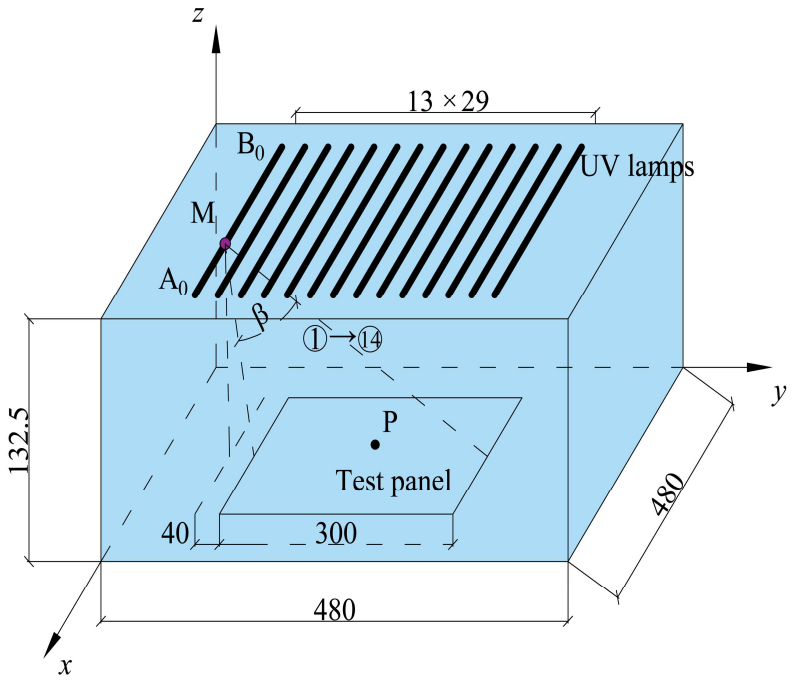



**Figure 6.** UV lamp radiation flux calculation model (Units: mm).

The other parameters in Equation (10) were given as follows:

$$I = \frac{\Phi h_0}{4\pi L \sin^2(\frac{\beta}{2})} \tag{11}$$

$$\beta = \arctan(\frac{340}{132.5}) - \arctan(\frac{40}{132.5}) \tag{12}$$

$$\cos \alpha = \frac{h_0}{d} \tag{13}$$

$$d = \sqrt{(x - x_m)^2 + (y - y_m)^2 + h_0^2} \tag{14}$$

where $I$ represents the UV lamp radiation intensity (W/sr), $\Phi$ denotes the UV light flux (W), $\beta$ is the angle between the radiation light and the nearest and furthest edge of the specimen, $l_0$ is the length of the UV lamp (m), $\alpha$ is the angle formed between the UV lamp radiation ray and its plumb line, $h_0$ is the distance between the UV lamp and the specimen (m), and $d$ is the distance between any point on the UV lamp and any point on the specimen (m).

The Equation (15) was used to determine the magnitude of UV radiation flux on the surface of the nano-$TiO_2$ cement slurry specimen:

$$E = \iint \frac{\Phi h_0^2}{4\pi d^3 L \sin^2(\beta/2)} dxdy \quad (15)$$

We incrementally activated two additional UV lamps at a time, starting from the center and extending towards both sides. Subsequently, we used MATLAB software to calculate the illuminance for various light configurations. Figure 7 illustrates how the efficiency of $NO_2$ photocatalytic degradation by nano-$TiO_2$ cement slurry is impacted by UV radiation flux. The efficiency of $NO_2$ photocatalytic degradation by nano-$TiO_2$ cement slurry increased as the UV radiation flux increased, ranging from 4.5 W/m$^2$ (with 2 UV lamps turned on) to 23.8 W/m$^2$ (with 10 UV lamps turned on). However, beyond a certain threshold, the degradation efficiency showed a declining trend. Under laboratory conditions, the optimal UV radiation flux was approximately 23.7 W/m$^2$, resulting in a degradation efficiency of around 35.6% as indicated by the fitting curve.

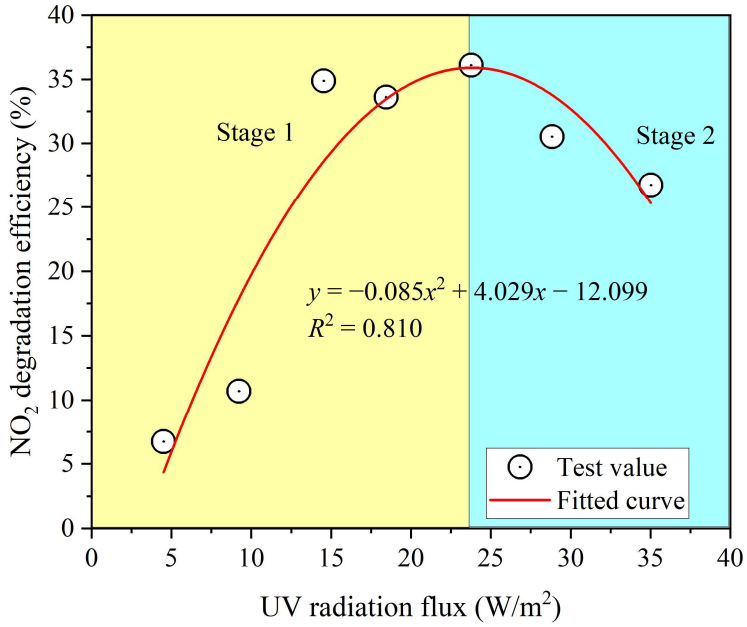



**Figure 7.** $NO_2$ degradation efficiency versus UV radiation flux.

As the number of activated UV lamps increased, the UV radiation flux directed at the nano-$TiO_2$ cement slurry and the excitation energy also increased. Consequently, the electron–hole pairs generated by nano-$TiO_2$ separated upon excitation, leading to improved photocatalytic degradation efficiency [50]. Previous studies have also shown similar effects of UV radiation flux on the degradation rate of $NO_x$ [53,54]. However, this increase in UV radiation flux resulted in a higher temperature of the reaction chamber and a decrease in humidity. When 10 UV lamps were activated, the temperature within the reaction chamber reached 31.2 °C, exceeding the optimal reaction temperature 28.8 °C. Additionally, the humidity level dropped to 59%, potentially falling below the required relative humidity. This could have diminished the generation of highly oxidative hydroxyl radicals. Thus, the efficiency of $NO_2$ photocatalytic degradation by nano-$TiO_2$ cement slurry decreased with an increase in UV radiation flux.

### *3.4. Effect of Thickness of Cement Slurry*

The thickness of the cement slurry specimens was measured individually using a vernier caliper with an index value of 0.02 mm. Each specimen was measured at four specific points, located at the midpoints of its four sides. The average of these measurements

was considered as the specimen's thickness value. To determine the actual thickness of the nano-$TiO_2$ cement slurry applied to the specimen's surface, we used a blank specimen without cement paste and measured its thickness. The difference between the thickness of the uncoated specimen and the measured thickness of the coated specimen provided the actual thickness of the nano-$TiO_2$ cement slurry layer applied. During the test, the six middle UV lamps were activated.

As shown in Figure 8, at different thicknesses of nano-$TiO_2$ cement slurry (1.00 mm, 3.72 mm, 4.02 mm, 6.10 mm, and 8.80 mm), the photocatalytic degradation efficiency of $NO_2$ by nano-$TiO_2$ cement slurry was 42.5 ± 0.6%, 40.0 ± 0.7%, 40.5 ± 2.0%, 40.7 ± 0.8%, and 39.9 ± 0.2%, respectively. The impact of nano-$TiO_2$ cement slurry thickness had little effect on $NO_2$ degradation efficiency. The photocatalytic process of nano-$TiO_2$ cement slurry mainly occurs at the gas–solid interface [22]. Increasing the thickness of the cement slurry could increase the total amount of nano-$TiO_2$. But the limited surface voids of the cement slurry resulted in a limited number of nano-$TiO_2$ that could come into direct contact with the $NO_2$. And most of the nano-$TiO_2$ was covered by the cement at the bottom of the surface layer and could not undergo the photocatalytic degradation reaction, as shown in Figure 2. Consequently, increasing the thickness of the nano-$TiO_2$ cement slurry does not seem to be a cost-effective method for improving degradation efficiency.

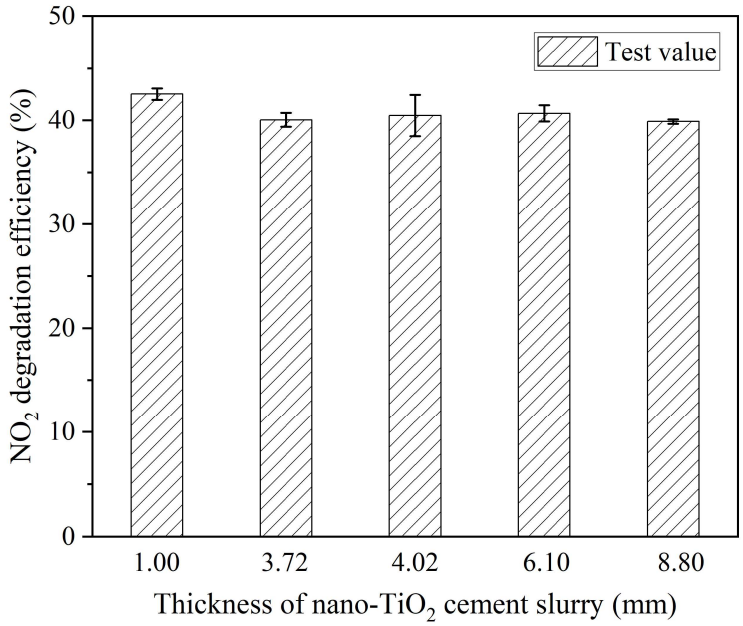



**Figure 8.** $NO_2$ degradation efficiency versus the thickness of cement slurry.

### *3.5. Effect of Amount of Dust Adhering to the Surface*

The coverage index (*c*) was utilized to quantify the impact of dust on the efficiency of $NO_2$ photocatalytic degradation by nano-$TiO_2$ cement slurry. It was calculated using Equation (18):

$$c = \frac{m}{s} \times 100\% \quad (16)$$

where m represents the amount of dust attached to the surface of the specimen (g), and s denotes the actual area of the specimen ($m^2$).

An appropriate quantity of loess was crushed into fine dust and then sieved through an aperture of 0.0075 $mm^2$. Subsequently, 5.71 g, 11.43 g, 22.86 g, 34.29 g, and 45.71 g of dust were precisely weighed using an electronic balance. The measured amounts of dust were then mixed with tap water in a mass ratio of 4:3 and thoroughly stirred. As shown in Figure 9, the dust slurry was uniformly applied to the surfaces of specimens B, C, D, E, and F, while specimen A remained blank.

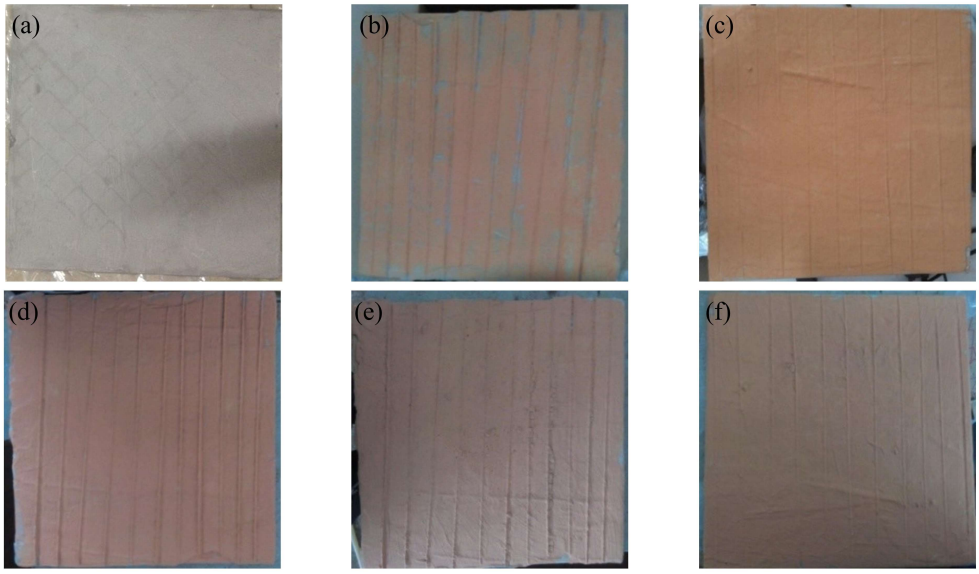



**Figure 9.** Specimens after dust adhesion: (**a**) specimen A; (**b**) specimen B; (**c**) specimen C; (**d**) specimen D; (**e**) specimen E; (**f**) specimen F.

As shown in Figure 10, the efficiency of $NO_2$ photocatalytic degradation by nano-$TiO_2$ cement slurry decreased as the coverage index increased, indicating a significant negative correlation between the two. Specifically, the degradation efficiency declined from 60.1 ± 1.8% to 40.9 ± 0.4% at a coverage index of 6.3. When the coverage index reached 50.8, the degradation efficiency plummeted to only 5.1 ± 0.2%, making its degradation capability nearly ineffective. This highlights the gas–solid nature of the photocatalytic degradation of nano-$TiO_2$, which mainly takes place on the surface of the nano-$TiO_2$ cement slurry and is significantly affected by the direct interaction between nano-$TiO_2$ and $NO_2$, as depicted in Figure 2 [22]. The presence of dust on the specimen's surface obstructed the available surface voids and hindered direct contact between nano-$TiO_2$ and $NO_2$. Consequently, it significantly adversely impacted the efficiency of $NO_2$ photocatalytic degradation by nano-$TiO_2$ cement slurry.

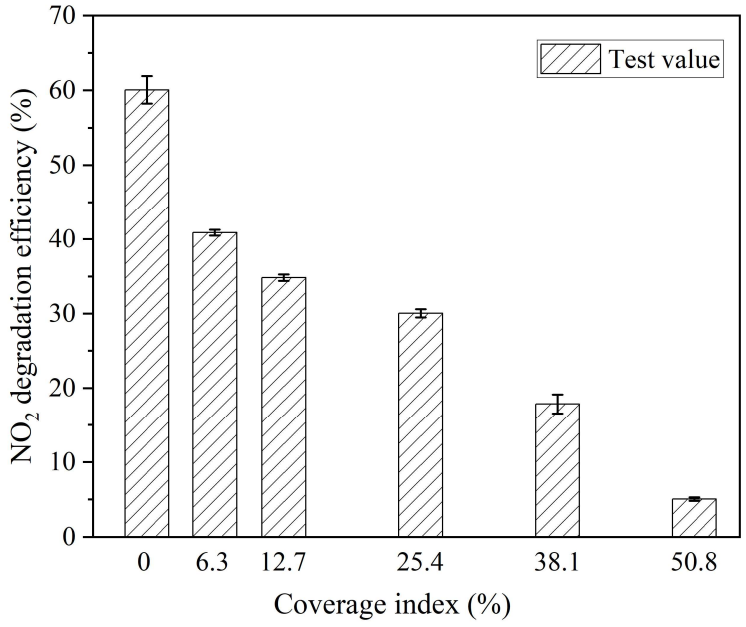



**Figure 10.** $NO_2$ degradation efficiency versus coverage index.

### *3.6. Effect of Number of Water Rinsing Cycles*

The maximum annual average rainfall in Changsha is approximately 1800 mL. We conducted tests by rinsing the specimen using a nozzle connected to a tap water pipe. When the water reached 1800 mL within 5 min, the valve on the water pipe was closed, and this was recorded as one rinsing cycle. Figure 11 illustrates the effect of the number of water rinsing cycles on the efficiency of $NO_2$ photocatalytic degradation by nano-$TiO_2$ cement slurry. Overall, the degradation efficiency decreased as the number of rinsing cycles increased. Specifically, the degradation efficiency decreased from 73.7 ± 0.7% to 54.1 ± 0.8% after two rinsing cycles (10 min). When the water rinsing cycles reached 10 (50 min), the degradation efficiency was further reduced to 49.9 ± 0.4%. This occurred because some of the nano-$TiO_2$ was washed off the surface during the rinsing process, resulting in a decrease in degradation efficiency. In a study of the literature [55], it was found that an abrasion resistance test of nano-$TiO_2$ cement slurry also indicated a decrease in $NO_x$ removal rate due to abrasion, similar to the result of water rinsing.

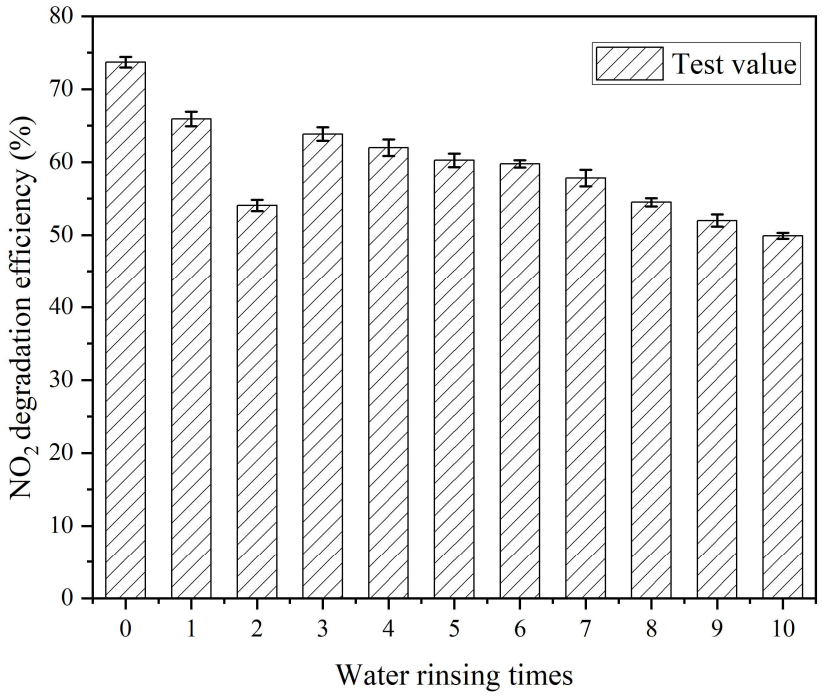



**Figure 11.** $NO_2$ degradation efficiency versus water rinsing cycles.

It is also worth noting that the efficiency of $NO_2$ photocatalytic degradation by nano-$TiO_2$ cement slurry recovered to 63.9% after three rinsing cycles (15 min). Initially, during the rinsing process, some nano-$TiO_2$ in the specimen was encapsulated by the cement slurry and unable to effectively participate in photocatalysis. As the rinsing progressed, the nano-$TiO_2$ concealed by the cement slurry gradually became exposed. With three rinsing cycles (15 min), the efficiency of $NO_2$ photocatalytic degradation by nano-$TiO_2$ cement slurry gradually improved. This observation emphasizes the importance of choosing panels with excellent adhesion to nano-$TiO_2$ cement slurry for practical engineering applications.

## 4. Experimental Details

### *4.1. Materials and Instruments*

In all tests, a commercially available nano-$TiO_2$ powder (titanium-type, average particle size = 10 nm) was used as the photocatalyst. Nano-$TiO_2$ cement slurry samples were prepared by mixing and stirring nano-$TiO_2$, silicate cement (425#), sodium tripolyphosphate (ACS 99%), and tap water. Table 1 summarizes the primary instruments and their associated parameters.

**Table 1.** Test instruments.

| Item | Photograph | Object | Range | Precision |
|---|---|---|---|---|
| FGA-4100 auto exhaust gas analyzer |  | NO | 0–5000 ppm | 1 ppm |
| HD-P900 nitrogen dioxide detector |  | $NO_2$ | 0–500 ppm | 0.01 ppm |
| Saipwell HG040-45W air heater |  | temperature | −45–80 °C | 0.1 °C |
| CSTH80 intelligent digital temperature and humidity controller |  | temperature and humidity | −19.9–99.9 °C<br>0.0–99.9% RH | 0.1 °C<br>0.1% RH |

### *4.2. Fabrication of Nano-$TiO_2$ Cement Slurry*

The mass proportion used for mixing the nano-$TiO_2$ cement slurry sample was 1:0.5:0.08:0.0024 (cement:water:nano-$TiO_2$:dispersant). Figure 12 illustrates the fabrication process of a nano-$TiO_2$ cement slurry sample [33]. First, a 3% sodium tripolyphosphate solution was prepared by dissolving it in tap water to serve as the dispersant solution. Next, the measured amount of nano-$TiO_2$ powder was added to the dispersant solution and stirred using a glass rod. The resulting mixture was then placed in an ultrasonic cleaner with a water bath for 20 min to ensure a uniform dispersion of the $TiO_2$ nanoparticles. Subsequently, the measured amount of cement was added to the dispersed nano-$TiO_2$ solution and stirred in the cement slurry mixer for 5 min. The well-stirred slurry was applied to a panel with dimensions of 300 × 300 × 8 mm and cured under standard conditions for 28 days.

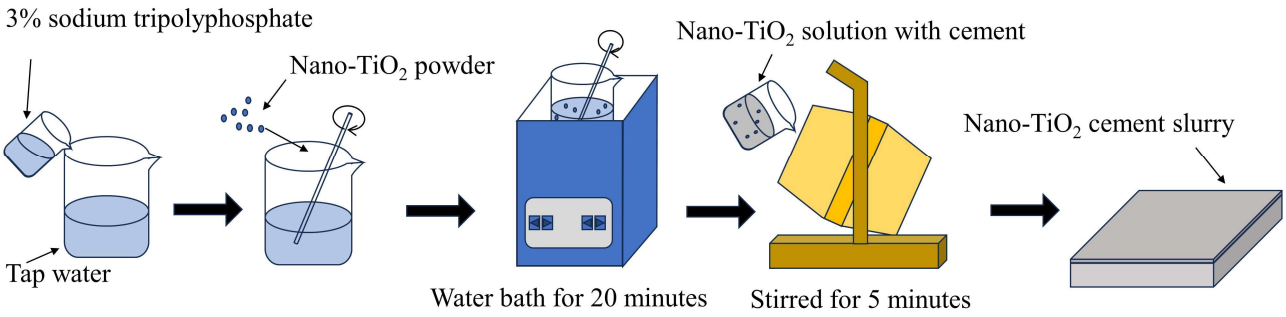



**Figure 12.** Fabrication process of nano-$TiO_2$ cement slurry sample.

### *4.3. Degradation of Vehicle Exhaust Test*

We independently developed a system for conducting vehicle exhaust degradation tests, as depicted in Figure 13. A reaction chamber with dimensions of 500 × 500 × 400 mm was constructed using 10 mm thick organic glass. To facilitate the photocatalytic degradation of vehicle exhaust in the cement slurry, fourteen identical UV lamps were used as energy sources for photocatalytic excitation. Each lamp had a spectrum, power, and length of 365 nm, 15 W, and 30 cm, respectively. The UV lamps were securely mounted on a steel frame, maintaining a distance of over 1 cm between the steel frame and the top plate of the reaction chamber to minimize the impact of the heat generated by the UV lamps on the temperature inside the chamber. To prevent the accumulation of exhaust fumes, a fan was attached to a foam board holding the test sample.

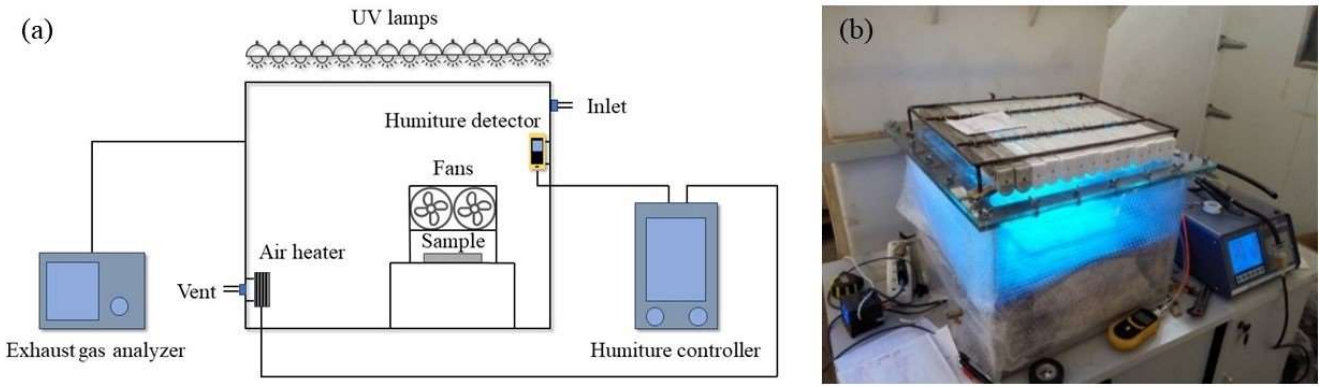



**Figure 13.** Vehicle exhaust test system: (**a**) schematic diagram; (**b**) site photo.

When conducting the experiment, the well-cured samples were initially placed inside the exhaust reaction chamber. Subsequently, pre-collected automotive exhaust was introduced into the reaction chamber, and the UV light source was activated to initiate the photocatalytic reaction. The total reaction time was 120 min, and data readings were taken every 20 min. During the vehicle exhaust test, temperature and humidity levels were controlled using an air heater and a temperature and humidity controller. Changes in vehicle exhaust concentration were monitored using a vehicle exhaust analyzer and a nitrogen dioxide detector connected to the reaction chamber.

### *4.4. Degradation Efficiency Evaluation Index*

The effectiveness of the photocatalytic cement slurry in degrading vehicle exhaust was assessed by measuring the reduction of vehicle exhaust concentration in the reaction chamber. The degradation efficiency for $NO_x$, denoted as $\omega_0$, was used as the evaluation index and calculated using Equation (17) [38–40]:

$$\omega_0 = \frac{(C_0 - C_1)}{C_0} \times 100\% \quad (17)$$

where $C_0$ and $C_1$ are the concentrations of $NO_x$ at the beginning and end of the reaction, respectively (ppm).

During the test, it was observed that some of the NO reacted with oxygen to produce $NO_2$, and a portion of the $NO_2$ in the vehicle exhaust test system was adsorbed onto the cement slurry surface. Consequently, we conducted a calibration test to determine the natural degradation efficiency of vehicle exhaust. Pure cement slurry without nano-$TiO_2$ was exposed to various initial concentrations of $NO_2$, and then the middle six UV lamps were turned on. Figure 14 illustrates the impact of initial concentrations on the removal ratio of $NO_2$. When the initial concentration of $NO_2$ in vehicle exhaust was 660 ppm or less, there was a positive correlation between its initial concentration and the removal ratio, with a correlation coefficient of 0.999. However, when the initial concentration of $NO_2$ exceeded

660 ppm, the removal ratio of $NO_2$ did not increase and remained constant at 54.78%. The rough, multi-void structure of cement slurry allows its surface to absorb some of the $NO_2$ gas. As the $NO_2$ concentration increased, more $NO_2$ was adsorbed, but the total amount of $NO_2$ adsorbed by the cement slurry remained constant. When the surface adsorption site was fully occupied, the removal ratio of $NO_2$ was not increased, but maintained at a stable level.

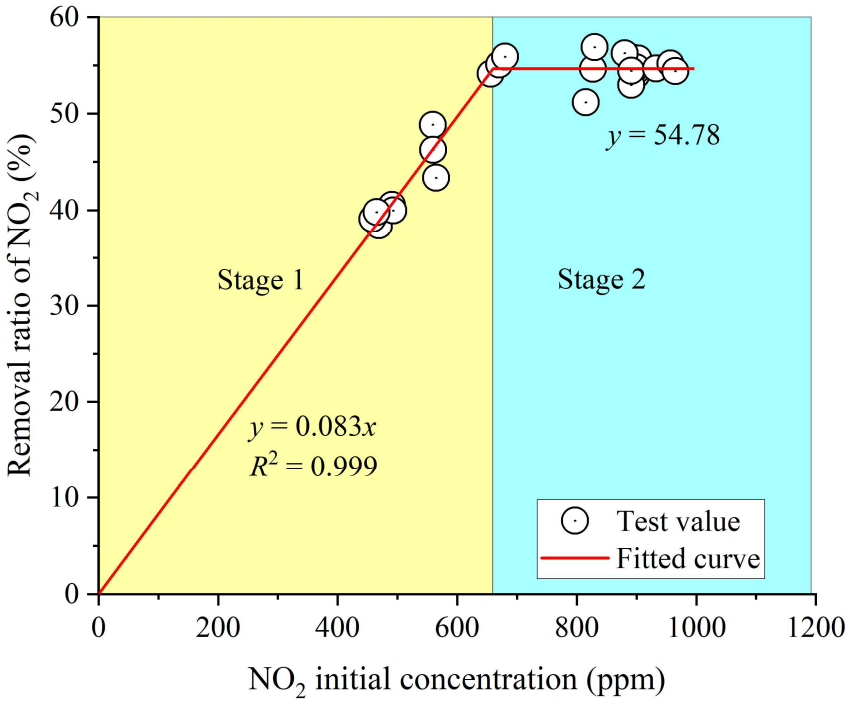



**Figure 14.** Relationship between the initial concentration and natural removal ratio of $NO_2$.

Considering the variation in $NO_2$ concentration within the reaction space of the vehicle exhaust test system, the calibrated degradation efficiency $\omega_1$ (Equation (18)) was used as the evaluation index for assessing the efficiency of $NO_2$ photocatalytic degradation by nano-$TiO_2$ cement slurry in the following evaluations:

$$\omega_1 = \frac{a \times (1-b) - c}{a \times (1-b)} \times 100\% \quad (18)$$

where $a$ is the initial concentration of $NO_2$ (ppm) and $b$ is the natural removal ratio of $NO_2$ concentration (ppm). If the initial concentration of $NO_2$ is more than 660 ppm, $b$ = 54.78%; otherwise, $b = 0.083 \times a$; $c$ is the concentration of $NO_2$ remaining after the reaction (ppm).

## 5. Field Application of Nano-$TiO_2$ Cement Slurry

Nano-$TiO_2$ cement slurry is used to degrade harmful components, such as $NO_2$ in vehicle exhaust. Most current assessments of the performance of nano-$TiO_2$ cement slurry photocatalytic materials in degrading vehicle exhaust use on-site instruments to measure changes in nitrogen oxide concentration [56]. However, the concentration of $NO_2$ in the field is influenced by natural environmental factors such as temperature, humidity, and wind speed. As a result, the test results may not accurately reflect the photocatalytic effectiveness of nano-$TiO_2$ materials. In this section, we introduce an evaluation method based on photocatalytic products to assess the performance of nano-$TiO_2$ cement slurry in the degradation of vehicle exhaust.

### *5.1. Field Application of Nano-$TiO_2$ Cement Slurry*

Test specimens (dimensions: 300 × 300 × 8 mm) coated with nano-$TiO_2$ cement slurry were prepared following the processing method presented in Figure 12. The cured test pieces were placed near the exit of an expressway toll station in Changsha for 8 days. Weather statistics for the period are presented in Table 2, and an on-site photo is shown in Figure 15. After 8 days, the test pieces were retrieved and rinsed with tap water using a sprayer, and the water used for rinsing was collected in a measuring cylinder. The concentration of $NO_3^-$ in the rinsing solution was determined using UV spectrophotometry [57].

**Table 2.** Weather statistics.

| Test Days | Weather | Temperature (°C) | Relative Humidity (%) |
|---|---|---|---|
| Day 1 | sunny to cloudy | 3–15 | 63 |
| Day 2 | cloudy | 6–10 | 70 |
| Day 3 | sunny to cloudy | 5–12 | 64 |
| Day 4 | cloudy | 5–13 | 59 |
| Day 5 | cloudy | 8–12 | 54 |
| Day 6 | sunny | 4–15 | 66 |
| Day 7 | sunny | 6–15 | 52 |
| Day 8 | sunny to cloudy | 6–17 | 47 |



**Figure 15.** Nano-$TiO_2$ cement slurry sample application field photo.

### *5.2. Determination of Optimal Rinsing Water Consumption*

Prior to the test, it was necessary to determine the amount of water needed to rinse the specimen. Insufficient water would result in $NO_3^-$ residues on the specimen's surface, hindering complete removal. Conversely, excessive water consumption would lead to a low concentration of $NO_3^-$ in the rinsing solution. The vehicle exhaust test system was set up to simulate the field environment. After 120 min, the test pieces were removed, washed with tap water, and the rinsing solution was collected. The concentration of $NO_3^-$ was determined using UV spectrophotometry. The relationship between $NO_3^-$ concentration and rinsing water consumption is shown in Figure 16. It was observed that, when the water consumption for rinsing the test panel was 25 mL, the $NO_3^-$ concentration in the resulting rinsing solution reached its peak at 6.48 mg/L.

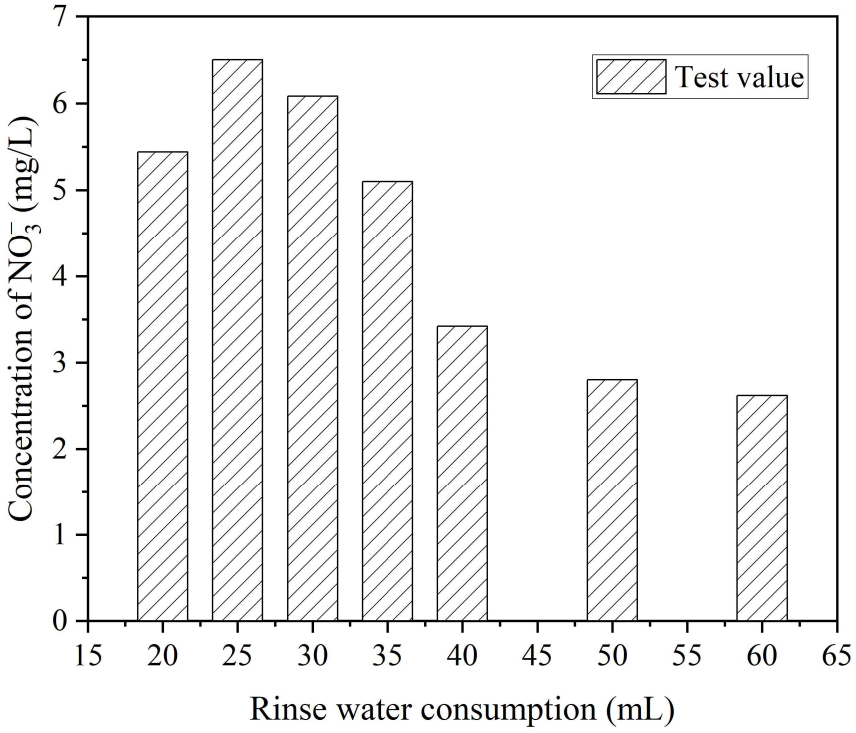



**Figure 16.** $NO_3^-$ concentration versus rinse water consumption.

*5.3. Evaluation of the Performance of Nano-$TiO_2$ Cement Slurry for Field Application*

The specimens placed in the field were retrieved and rinsed by spraying them with tap water. A measuring cylinder was used to collect the rinsing solution, and the rinsing was stopped when the collected solution reached 25 mL. The average concentration of $NO_3^-$ in the rinsing solution was 10.85 mg/L as determined by UV spectrophotometry. The $NO_3^-$ content in the rinsing solution was 0.27125 mg, calculated by multiplying the concentration of $NO_3^-$ by the volume of the collected 25 mL rinsing water. It was further calculated that the amount of $NO_2$ degraded in vehicle exhaust by the nano-$TiO_2$ sample was 0.20125 mg. By dividing the panel placement time and area, the $NO_2$ photocatalytic degradation efficiency by the nano-$TiO_2$ specimen was approximately 0.28 mg/$m^2$/day.

## 6. Conclusions

The aim of this study was to examine the impact of various environmental factors on the efficiency of $NO_2$ photocatalytic degradation by nano-$TiO_2$ cement slurry, and to assess its practical applicability. The nano-$TiO_2$ cement slurry was prepared using the ultrasonic dispersion method. Subsequently, a vehicle exhaust test system was established, and a new index for evaluating degradation efficiency was determined to investigate the experimental variables. Finally, the effectiveness of using nano-$TiO_2$ cement slurry for the photocatalytic degradation of vehicle exhaust was assessed at an expressway toll station. Based on the results, the following conclusions can be drawn:

(1) The efficiency of $NO_2$ photocatalytic degradation by nano-$TiO_2$ cement slurry was significantly affected by temperature and UV illumination. There was an optimal temperature (28.8 °C in this test) at which the degradation efficiency was maximized. As the temperature increased, the degradation efficiency initially increased and then declined.

(2) Excessive water molecules and dust on the cement surface will compete with $NO_2$ for adsorption on nano-$TiO_2$, thereby occupying specific active sites of the catalyst. Consequently, an increase in relative humidity (falling within the range of 64.1% to 81.8%) results in a reduced degradation efficiency of nano-$TiO_2$ cement slurry for $NO_2$.

(3) The thickness of the nano-$TiO_2$ cement slurry had only a minor impact on the efficiency of $NO_2$ photocatalytic degradation by nano-$TiO_2$ cement slurry. The photocatalytic properties of the samples were significantly diminished by surface dust and rain erosion.

(4) The evaluation method based on photocatalytic products for assessing the photocatalytic performance of nano-$TiO_2$ cement slurry in degrading vehicle exhaust is less affected by natural environmental factors. Field application has shown that the nano-$TiO_2$ cement paste exhibits good performance in the photocatalytic degradation of vehicle exhaust. The efficiency of $NO_2$ photocatalytic degradation by nano-$TiO_2$ cement slurry was approximately 0.28 $mg/m^2/day$.

In field applications, the current cost of laying nano-$TiO_2$ cement slurry is relatively high. However, with the advancement of nano-$TiO_2$ preparation technology and market development, the cost is expected to be significantly reduced. At the same time, the bonding of nano-$TiO_2$ cement slurry to road accessory materials is an important factor affecting the large-scale application of nano-$TiO_2$ cement slurry. How to make nano-$TiO_2$ cement slurry effectively bonded with road accessory materials is an important research direction for the future.

**Author Contributions:** Conceptualization, Formal analysis, Methodology, Funding acquisition, Writing—review and editing, Y.K.; Formal analysis, Data curation, Investigation, Methodology, Writing—original draft, F.D.; Investigation, Writing—original draft, Writing—review and editing, Z.P.; Writing—original draft, F.F.; Data curation, Z.Z.; Funding acquisition, X.J. All authors have read and agreed to the published version of the manuscript.

**Funding:** This research work was funded by the National Natural Science Foundation of China (Grant No. 52378210 and 51878663), the Natural Science Foundation of Hunan Province, China (Grant No. 2023JJ30674), and Fundamental Research Funds for Central Universities of Central South University (Grant No. 2023ZZTS0408).

**Data Availability Statement:** The data that support the findings of this study are available from the corresponding author (Z.P.) upon reasonable request.

**Conflicts of Interest:** Zhaohuan Zhang is employed in the Economic and Technical Research Institute of State Grid Shandong Electric Power Company. The remaining authors declare no conflicts of interest.

## References

1. Zhang, T.; Jin, T.; Qi, J.; Liu, S.; Hu, J.; Wang, Z.; Li, Z.; Mao, H.; Xu, X. Influence of test cycle and fuel property on fuel consumption and exhaust emissions of a heavy-duty diesel engine. *Energy* **2022**, *244*, 122705. [CrossRef]
2. Marques, B.; Kostenidou, E.; Valiente, A.M.; Vansevenant, B.; Sarica, T.; Fine, L.; Temime-Roussel, B.; Tassel, P.; Perret, P.; Liu, Y.; et al. Detailed Speciation of Non-Methane Volatile Organic Compounds in Exhaust Emissions from Diesel and Gasoline Euro 5 Vehicles Using Online and Offline Measurements. *Toxics* **2022**, *10*, 184. [CrossRef] [PubMed]
3. Zhang, Z.; Liu, K.; Chong, D.; Niu, D.; Lin, P.; Liu, X.; Niu, Y.; Jing, R. Evaluation of photocatalytic micro-surfacing mixture: Road performance, vehicle exhaust gas degradation capacity and environmental impacts. *Constr. Build. Mater.* **2022**, *345*, 128367. [CrossRef]
4. Zhu, Y.; Pan, Z.; Jing, D.; Liang, H.; Cheng, J.; Li, D.; Zhou, X.; Lin, F.; Liu, H.; Pan, P.; et al. Association of air pollution, genetic risk, and lifestyle with incident adult-onset asthma: A prospective cohort study. *Ecotoxicol. Environ. Saf.* **2023**, *257*, 114922. [CrossRef] [PubMed]
5. Bronte, O.; García-García, F.; Lee, D.-J.; Urrutia, I.; Uranga, A.; Nieves, M.; Martínez-Minaya, J.; Quintana, J.M.; Arostegui, I.; Zalacain, R.; et al. Impact of outdoor air pollution on severity and mortality in COVID-19 pneumonia. *Sci. Total Environ.* **2023**, *894*, 164877. [CrossRef] [PubMed]
6. Tyukavkina, V.V.; Shchelokova, E.A.; Tsyryatyeva, A.V.; Kasikov, A.G. $TiO_2$–$SiO_2$ nanocomposites from technological wastes for self-cleaning cement composition. *J. Build. Eng.* **2021**, *44*, 102648. [CrossRef]
7. Bej, D.; Chattaraj, N. Air pollution from vehicle-tailpipe emissions and diagnostic approaches through cyber–physical platform—A review. *Microprocess. Microsyst.* **2023**, *98*, 104805. [CrossRef]
8. Pérez-Nicolás, M.; Navarro-Blasco, I.; Fernández, J.M.; Alvarez, J.I. Atmospheric $NO_x$ removal: Study of cement mortars with iron- and vanadium-doped $TiO_2$ as visible light–sensitive photocatalysts. *Constr. Build. Mater.* **2017**, *149*, 257–271. [CrossRef]

9. Huang, M.; Huang, Y.; Cao, J.; Tao, W. Study on mitigation of automobile exhaust pollution in an urban street canyon: Emission reduction and air cleaning street lamps. *Build. Environ.* **2021**, *193*, 107651. [CrossRef]
10. Paul, L.A.; Burnett, R.T.; Kwong, J.C.; Hystad, P.; Donkelaar, A.; Bai, L.; Goldberg, M.S.; Lavigne, E.; Copes, R.; Martin, R.V.; et al. The impact of air pollution on the incidence of diabetes and survival among prevalent diabetes cases. *Environ. Int.* **2020**, *134*, 105333. [CrossRef]
11. Tamayo, T.; Rathmann, W.; Stahl-Pehe, A.; Landwehr, S.; Sugiri, D.; Krämer, U.; Hermann, J.; Holl, R.; Rosenbauer, J. No adverse effect of outdoor air pollution on HbA1c in children and young adults with type 1 diabetes. *Int. J. Hyg. Environ. Health* **2016**, *219*, 349–355. [CrossRef] [PubMed]
12. Li, X.; Zhang, L.; Li, L.; Hu, Y.; Liu, J.; Xu, Y.; Luo, C.; Zheng, C. NO removal from flue gas using conventional imidazolium-based ionic liquids at high pressures. *Energy Fuels* **2018**, *32*, 6039–6048. [CrossRef]
13. Huang, R.-J.; Zhang, Y.; Bozzetti, C.; Ho, K.-F.; Cao, J.-J.; Han, Y.; Daellenbach, K.R.; Slowik, J.G.; Platt, S.M.; Canonaco, F.; et al. High secondary aerosol contribution to particulate pollution during haze events in China. *Nature* **2014**, *514*, 218–222. [CrossRef] [PubMed]
14. Mochida, I.; Korai, Y.; Shirahama, M.; Kawano, S.; Hada, T.; Seo, Y.; Yoshikawa, M.; Yasutake, A. Removal of $SO_x$ and $NO_x$ over activated carbon fibers. *Carbon* **2000**, *38*, 227–239. [CrossRef]
15. Hooftman, N.; Messagie, M.; Joint, F.; Segard, J.-B.; Coosemans, T. In-life range modularity for electric vehicles: The environmental impact of a range-extender trailer system. *Appl. Sci.* **2018**, *8*, 1016. [CrossRef]
16. Venu, H.; Subramani, L.; Dhana, R.V. Emission reduction in a DI diesel engine using exhaust gas recirculation (EGR) of palm biodiesel blended with $TiO_2$ nano additives. *Renew. Energy* **2019**, *140*, 245–263. [CrossRef]
17. Li, R.; Wu, J.; Liu, H.; Gao, Z.; Sun, H.; Ding, R.; Tang, T. Crowded urban traffic: Co-evolution among land development, population, roads and vehicle ownership. *Nonlinear Dyn.* **2019**, *95*, 2783–2795. [CrossRef]
18. Lapidus, A.; Korolev, E.; Topchiy, D.; Kuzmina, T.; Shekhovtsova, S.; Shestakov, N. Self-cleaning cement-based building materials. *Buildings* **2022**, *12*, 606. [CrossRef]
19. Zhang, Z.; Tan, J.; Cheng, L.; Yang, W. Carbon nano-layer coated $TiO_2$ nanoparticles for efficient photocatalytic $CO_2$ reduction into $CH_4$ and CO. *Ceram. Int.* **2021**, *47*, 34106–34114. [CrossRef]
20. Qian, G.; Yu, H.; Gong, X.; Zhao, L. Impact of Nano-$TiO_2$ on the $NO_2$ degradation and rheological performance of asphalt pavement. *Constr. Build. Mater.* **2019**, *218*, 53–63. [CrossRef]
21. Li, R.; Xiao, F.; Amirkhanian, S.; You, Z.; Huang, J. Developments of nano materials and technologies on asphalt materials—A review. *Constr. Build. Mater.* **2017**, *143*, 633–648. [CrossRef]
22. Jia, Z.; Zhao, Y.; Shi, J. Adsorption kinetics of the photocatalytic reaction of nano-$TiO_2$ cement-based materials: A review. *Constr. Build. Mater.* **2023**, *370*, 130462. [CrossRef]
23. Nada, A.A.; El Rouby, W.M.A.; Bekheet, M.F.; Antuch, M.; Weber, M.; Miele, P.; Viter, R.; Roualdes, S.; Millet, P.; Bechelany, M. Highly textured boron/nitrogen co-doped $TiO_2$ with honeycomb structure showing enhanced visible-light photoelectrocatalytic activity. *Appl. Surf. Sci.* **2020**, *505*, 144419. [CrossRef]
24. Guo, M.; Poon, C. Photocatalytic NO removal of concrete surface layers intermixed with $TiO_2$. *Build. Environ.* **2013**, *70*, 102–109. [CrossRef]
25. Dylla, H.; Hassan, M.M.; Osborn, D. Field evaluation of photocatalytic concrete pavements' ability to remove nitrogen oxides. *Trans. Res. Rec.* **2012**, *2290*, 154–160. [CrossRef]
26. Shen, S.; Burtou, M.; Jobson, B.; Haselbach, L. Pervious concrete with titanium dioxide as a photocatalyst compound for a greener urban road environment. *Constr. Build. Mater.* **2012**, *35*, 874–883. [CrossRef]
27. Xia, H.; Liu, G.; Zhang, R.; Song, L.; Chen, H. The Photocatalytic Degradation of Vehicle Exhausts by an Fe/N/Co–$TiO_2$ Waterborne Coating under Visible Light. *Materials* **2019**, *12*, 3378. [CrossRef]
28. Witkowski, H.; Jarosławski, J.; Tryfon-Bojarska, A. Application of Photocatalytic Concrete Paving Blocks in Poland—Verification of Effectiveness of Nitric Oxides Reduction and Novel Test Method. *Materials* **2020**, *13*, 5183. [CrossRef]
29. Wang, Y.; Wang, X.; Niu, D.; Niu, Y.; Xia, H.; Wang, Y. Effect of Photocatalyst on Rheological Behavior and NO Degradation Capacity of Asphalt Binder. *Catalysts* **2023**, *13*, 1083. [CrossRef]
30. Bhattu, M.; Singh, J. Recent advances in nanomaterials based sustainable approaches for mitigation of emerging organic pollutants. *Chemosphere* **2023**, *321*, 138072. [CrossRef]
31. Das, S.; Mukherjee, A. Chapter 1—Nanotechnology as sustainable strategy for remediation of soil contaminants, air pollutants, and mitigation of food biodeterioration. In *Environmental Applications of Microbial Nanotechnology*; Elsevier: Amsterdam, The Netherlands, 2023; pp. 3–16. [CrossRef]
32. Qian, C.; Zhao, L.; Wang, R. Effect of concentration of nitrogen oxidizes on photocatalytic oxidation efficiency of nano-$TiO_2$ photocatalyst immobilized on cement-based material. *Mater. Sci. Technol.* **2007**, *15*, 582–585. (In Chinese)
33. Luo, G.; Liu, H.; Li, W.; Lyu, X. Automobile Exhaust Removal Performance of Pervious Concrete with Nano $TiO_2$ under Photocatalysis. *Nanomaterials* **2020**, *10*, 2088. [CrossRef] [PubMed]
34. Jin, J.; Chen, B.; Liu, L.; Liu, R.; Qian, G.; Wei, H.; Zheng, J. A Study on Modified Bitumen with Metal Doped Nano-$TiO_2$ Pillared Montmorillonite. *Materials* **2019**, *12*, 1910. [CrossRef] [PubMed]
35. Kuang, Y.; Zhang, Z.; Ji, X.; Zhang, X. Study on nano-$TiO_2$ photocatalytic cement paste with of automobile exhaust degradation performance. *J. Funct. Mater.* **2017**, *48*, 2241–2246. (In Chinese) [CrossRef]

36. Jin, J.; Xiao, T.; Tan, Y.; Zheng, J.; Liu, R.; Qian, G.; Wei, H.; Zhang, J. Effects of $TiO_2$ pillared montmorillonite nanocomposites on the properties of asphalt with exhaust catalytic capacity. *J. Clean. Prod.* **2018**, *205*, 339–349. [CrossRef]
37. Saber, N.B.; Mezni, A.; Alrooqi, A.; Altalhi, T. Fabrication of efficient Au@$TiO_2$/rGO heterojunction nanocomposite: Boosted photocatalytic activity under ultraviolet and visible light irradiation. *J. Mater. Res. Technol.* **2021**, *12*, 2238–2246. [CrossRef]
38. Guo, M.; Chen, J.; Xia, M.; Wang, T.; Poon, C. Pathways of conversion of nitrogen oxides by nano $TiO_2$ incorporated in cement-based materials. *Build. Environ.* **2018**, *144*, 412–418. [CrossRef]
39. Liu, S.; Shi, Z. Study on catalytic decomposition of vehicle exhaust pavement materials by $TiO_2$. *Energy Rep.* **2022**, *8*, 161–170. [CrossRef]
40. Chen, C.; Tang, B.; Cao, X.; Gu, F.; Huang, W. Enhanced photocatalytic decomposition of NO on portland cement concrete pavement using nano-$TiO_2$ suspension. *Constr. Build. Mater.* **2021**, *275*, 122135. [CrossRef]
41. Xie, J.; Kuang, Y. Photocatalytic technology of nano-$TiO_2$ and its application in photodegradation of automobile exhaust. *Mater. Rep.* **2012**, *26*, 141–145. (In Chinese) [CrossRef]
42. Li, X.; Wang, F.; You, L.; Wu, S.; Yang, C.; Zhang, L.; Barbieri, D.M. A review on photocatalytic asphalt pavement designed for degradation of vehicle exhausts. *Transp. Res. D Transp. Environ.* **2023**, *115*, 103605. [CrossRef]
43. Fan, W.; Chan, K.; Zhang, C.; Leung, M.K.H. Advanced solar photocatalytic asphalt for removal of vehicular $NO_x$. *Energy Procedia* **2017**, *143*, 811–816. [CrossRef]
44. Zhang, L.; Lu, Q.; Shan, R.; Zhang, F.; Muhammad, Y.; Huang, K. Photocatalytic degradation of vehicular exhaust by nitrogen-doped titanium dioxide modified pavement material. *Transp. Res. D Transp. Environ.* **2021**, *91*, 102690. [CrossRef]
45. Ballari, M.M.; Yu, Q.L.; Brouwers, H.J.H. Experimental study of the NO and $NO_2$ degradation by photocatalytically active concrete. *Catal. Today* **2011**, *161*, 175–180. [CrossRef]
46. Lin, Y.T.; Weng, C.H.; Chen, F.Y. Key operating parameters affecting photocatalytic activity of visible-light-induced C-doped $TiO_2$ catalyst for ethylene oxidation. *Chem. Eng. J.* **2014**, *248*, 175–183. [CrossRef]
47. Xiao, L.; Chen, P.; Yang, W.; Zhao, X.; Dong, F. Photocatalytic reaction mechanisms at the gas–solid interface for environmental and energy applications. *Catal. Sci. Technol.* **2021**, *11*, 7807–7839. [CrossRef]
48. Hager, S.; Bauer, R.; Kudielka, G. Photocatalytic oxidation of gaseous chlorinated organics over titanium dioxide. *Chemosphere* **2000**, *41*, 1219–1225. [CrossRef]
49. Sánchez, B.; Cardona, A.I.; Romero, M.; Avila, P.; Bahamonde, A. Influence of temperature on gas-phase photo-assisted mineralization of TCE using tubular and monolit. *Catal. Today* **1999**, *54*, 369–377. [CrossRef]
50. Qian, C.; Zhao, L.; Fu, D.; Li, L.; Wang, R. Study on the effect of temperature, humidity and light intensity on photocatalytic oxidation of $NO_2$ by Nano-$TiO_2$ immobilized on cement-based materials. *Acta Sci. Circumstantiae* **2005**, *25*, 623–630. (In Chinese) [CrossRef]
51. Pellegrino, F.; Zangirolami, M.; Minero, C.; Maurino, V. Portable photoreactor for on-site measurement of the activity of photocatalytic surfaces. *Catal. Today* **2020**, *340*, 363–368. [CrossRef]
52. Casagrande, C.A.; Repette, W.L.; Hotza, D. Effect of environmental conditions on degradation of $NO_x$ gases by photocatalytic nanotitania-based cement mortars after long-term hydration. *J. Clean. Prod.* **2020**, *274*, 123067. [CrossRef]
53. Puddu, V.; Choi, H.; Dionysiou, D.D.; Li Puma, G. $TiO_2$ photocatalyst for indoor air remediation: Influence of crystallinity, crystal phase, and UV radiation intensity on trichloroethylene degradation. *Appl. Catal. B* **2010**, *94*, 211–218. [CrossRef]
54. Wang, K.H.; Tsai, H.H.; Hsieh, Y.H. A study of photocatalytic degradation of trichloroethylene in vapor phase on $TiO_2$ photocatalyst. *Chemosphere* **1998**, *36*, 2763–2773. [CrossRef]
55. Guo, M.Z.; Ling, T.C.; Poon, C.S. Photocatalytic $NO_x$ degradation of concrete surface layers intermixed and spray-coated with nano-$TiO_2$: Influence of experimental factors. *Cem. Concr. Compos.* **2017**, *83*, 279–289. [CrossRef]
56. Folli, A.; Strøm, M.; Madsen, T.P.; Henriksen, T.; Lang, J.; Emenius, J.; Klevebrant, T.; Nilsson, A. Field study of air purifying paving elements containing $TiO_2$. *Atmos. Environ.* **2015**, *107*, 44–51. [CrossRef]
57. *GB/T 5750.5-2023*; Standard Examination Methods for Drinking Water—Part 5: Inorganic Nonmetallic Indices. Standards Press of China: Beijing, China, 2023. (In Chinese)


**Disclaimer/Publisher's Note:** The statements, opinions and data contained in all publications are solely those of the individual author(s) and contributor(s) and not of MDPI and/or the editor(s). MDPI and/or the editor(s) disclaim responsibility for any injury to people or property resulting from any ideas, methods, instructions or products referred to in the content.